Tectonophysics xxx (2017) xxx–xxx

Contents lists available at ScienceDirect

Tectonophysics

journal homepage: www.elsevier.com/locate/tecto

Interactions of scales of convection in the Earth's mantle

Nicolas Coltice[a,*], Gaspard Larrouturou[a], Eric Debayle[a], Edward J. Garnero[b]

[a] Laboratoire de Géologie de Lyon, Université Claude Bernard Lyon 1, Ecole Normale Supérieure de Lyon, CNRS, France
[b] School of Earth and Space Exploration, Arizona State University, USA

ARTICLE INFO

Article history:
Received 27 January 2017
Received in revised form 16 June 2017
Accepted 25 June 2017
Available online xxxx

Keywords:
Mantle convection
Plate tectonics
Small scale convection
Seismology
Lithosphere

ABSTRACT

The existence of undulations of the geoid, gravity and bathymetry in ocean basins, as well as anomalies in heat flow, point to the existence of small scale convection beneath tectonic plates. The instabilities that could develop at the base of the lithosphere are sufficiently small scale (<500 km) that they remain mostly elusive from seismic detection. We take advantage of 3D spherical numerical geodynamic models displaying plate-like behavior to study the interaction between large-scale flow and small-scale convection. We find that finger-shaped instabilities develop at seafloor ages >60 Ma. They form networks that are shaped by the plate evolution, slabs, plumes and the geometry of continental boundaries. Plumes impacting the boundary layer from below have a particular influence through rejuvenating the thermal lithosphere. They create a wake in which new instabilities form downstream. These wakes form channels that are about 1000 km wide, and thus are possibly detectable by seismic tomography. Beneath fast plates, cold sinking instabilities are tilted in the direction opposite to plate motion, while they sink vertically for slow plates. These instabilities are too small to be detected by usual seismic methods, since they are about 200 km in lateral scale. However, this preferred orientation of instabilities below fast plates could produce a pattern of large-scale azimuthal anisotropy consistent with both plate motions and the large scale organisation of azimuthal anisotropy obtained from recent surface wave models.

1. Introduction

The theory of plate tectonics provides an explanation for the heat flow distribution in ocean basins. As the distance increases from mid-ocean ridges, heat flow decreases with age because plates are cooling (McKenzie, 1967). However, after about 50 My of cooling, heat flow seems to stabilize, as if a source of heat from below would maintain a thermal equilibrium at the base of plates (Parsons and Sclater, 1977). The continually increasing number of heat flow measurements still fits this pattern (Hasterok et al., 2011). Richter and Parsons (1975) proposed that two scales of convection operate in the mantle, a large-scale flow responsible for the generation and evolution of plates, which would be represented by the distance between ridges and subduction in a simple view, and a smaller-scale flow, which would exist beneath plates and would extend through the upper mantle only.

The large-scale convective system is supported by extensive observations and modeling: the most striking being tomographic evidence for it (Grand et al., 1997). Numerical convection models successfully capture this large-scale system, controlled by the existence of continents (Gurnis, 1988; Guillou and Jaupart, 1995), the presence of a viscosity jump in the mantle (Bunge et al., 1996; Zhong et al., 2000), and the strength of the lithosphere (Van Heck and Tackley, 2008; Foley and Becker, 2009; Mallard et al., 2016). The small-scale system is difficult to observe, but undulations of the geoid, gravity and bathymetry in the direction of plate motions, at scales between 200 km and 1000 km, constitute a strong case (Haxby and Weissel, 1986; Fleitout and Moriceau, 1992; Hayn et al., 2012). Because of the small extent and small values of the temperature anomalies, the seismic detection of this phenomenon is extremely difficult (Sleep, 2011). Resolution in seismic waveform tomography has improved enough to resolve range of heterogeneity wavelengths, which might be related to the development of small scale convection (French et al., 2013). Higher resolution seismic studies hold the greatest promise for detection of small-scale convective instabilities (Lin et al., 2016).

On the dynamical modeling side, extensive analytical, numerical and experimental studies characterize the conditions of onset of small-scale convection, its development, and its relationship with observations like melting (Boutilier and Keen, 1999; Ballmer et al., 2007). The age of the overlying oceanic plate were the onset of small-scale convection occurs directly depends on the viscosity contrast

* Corresponding author at: Université Claude Bernard Lyon 1, Laboratoire de Géologie de Lyon, Villeurbanne Cedex 68622, France.
E-mail address: coltice@univ-lyon1.fr (N. Coltice).

http://dx.doi.org/10.1016/j.tecto.2017.06.028
0040-1951/

through the lithosphere (Davaille and Jaupart, 1994; Korenaga and Jordan, 2003; Huang et al., 2003; Solomatov, 2004). The flow organisation in rolls parallel to plate motion proposed by Richter and Parsons (1975) is confirmed by 3D thermo-chemical calculations, although numerical models show that the geometry is more complex and articulated around moving finger-shaped instabilities (Marquart, 2001; van Hunen et al., 2005). The faster the plate velocity, the more aligned the networks of instabilities become (Sleep, 2011).

With the exception of the works of Korenaga and Jordan (2003) and Solomatov (2004) on the initiation of subduction by small-scale convection, the numerical studies display either only large-scale convection or only small-scale convection, but not the dynamic interactions between them. The present paper therefore explores and reports on results of global convection models in 3D spherical geometry where both scales of convection are present and interact. We describe the self-organisation of the multi-scale system and its relationship with plate motions, continents, slabs and plumes, and propose ways to detect the wake of plumes interacting with the lithosphere and small-scale convective patterns using seismology.

2. Method

In this section, we generate a model of flow and temperature at the present day in the Earth, imposing plate velocities at the surface of a convection model. We make strong assumptions on the physics and initial conditions of the modeling, especially for the deep mantle. However, we study here the dynamics of the top 700 km of the mantle. Therefore, approximations of initial conditions, compressibility and deep mantle material properties should have little effect on our findings. The specificity of this 3D spherical model is the extreme viscosity contrast across the lithosphere, that produces both large-scale and small-scale convection. Other studies have lower viscosity contrasts (Zhong et al., 2000; Zhang et al., 2010; Davies et al., 2012), and eventually force a stable temperature profile in the lithosphere (Bower et al., 2015), so they do not produce small-scale instabilities.

2.1. Physical and numerical model

We model the evolution of temperature, pressure and flow velocity in the Earth's mantle by an approximation of its dynamics. We compute numerical solutions of the equations of conservation of mass, momentum and energy, and advection of material properties, together with a pseudo-plastic rheology and a Boussinesq approximation for the equation of state. The physics of phase changes, compressibility, melting, deep dense chemical anomalies are neglected and the rheology is certainly simplified. However, such model is already at the limit of computational capabilities. We use the code StagYY (Tackley, 2008) to solve this set of equations in 3D spherical geometry over a Yin-Yang grid (Kageyama and Sato, 2004). The 2D version of the code is also benchmarked for pseudo-plasticity (Tosi et al., 2015). StagYY handles several orders of magnitude of viscosity contrasts between adjacent nodes (Tackley, 2008). The resolution here is 30 km on average, refined close to boundary layers in the vertical direction (10 km radial resolution close to the surface). Viscosity increases smoothly with depth by a factor of 20 according to an activation volume. We also impose a viscosity increase by a factor of 30 at 660 km, consistent with the radial viscosity structure of the Earth inferred from non-hydrostatic geoid anomalies (Ricard et al., 1993). However, recent studies point to a possible jump of the viscosity slightly deeper at 1000 km (Rudolph et al., 2015).

Viscosity is also thermally activated, following

$$\eta(z,T) = \eta_0(z)\ \exp\left(\frac{E_a}{RT}\right),$$

where E_a is the activation energy being 142 kJ mol^{-1}, R the gas constant and T the absolute dimensional temperature. The approximation here is to use a viscosity law appropriate for diffusion creep over the whole mantle. We therefore neglect dislocation creep and other deformation mechanisms at lower temperature. But diffusion creep with an activation energy lower than experimental values for olivine (500 kJ mol^{-1} (Idrissi et al., 2016)) decently mimics dislocation creep (Christensen, 1984; van Hunen et al., 2005). However, this lower activation energy is still lower by more than a factor of two than the expected value for diffusion creep in the lower mantle, where this deformation mechanism would dominate (Yamazaki and Karato, 2001). Accounting for the full complexity of mantle rheology in such 3D spherical models is a computational challenge, especially for large activation energies which produce extreme viscosity contrasts that are difficult to accurately resolve.

The reference viscosity of 1 corresponds to a temperature of 0.64 at zero pressure. This value is chosen arbitrarily and corresponds a priori (before the model is realised) to the expected temperature at the base of the upper boundary layer. To limit the viscosity variations, we set a cut-off for the maximum value of the viscosity at 10^4. Therefore, the viscosity contrast before the realisation of the model is expected to be 10^4 across the upper boundary layer. After the realisation, the average value of the temperature at the base of the upper boundary layer is hotter than expected a priori, being 0.75, but stable in the initial unconstrained stage and with imposed plate velocities (see next subsection). Therefore, the typical viscosity in the asthenospheric mantle is around 10^{-2} as seen from Fig. 1. On the horizontally averaged viscosity profile in Fig. 1, the influence of cold and stiff slabs smoothes out the viscosity jump at 660 km in a way the maximum laterally averaged viscosity in the deep mantle is reached at 1000 km.

We use a stress dependence of the viscosity through a pseudo-plastic approximation in order to produce plate boundaries surrounding strong plate interiors (see for instance Rolf et al., 2012). This choice leads to stiff slabs as described by Bello et al. (2015). Viscosity also depends on the type of material, which is tracked with markers. We use three types of materials. Ambient mantle corresponds to the largest fraction of the spherical shell. Continental nuclei are 175 km thick. They are buoyant, their buoyancy number being −0.4 (200 kg m^{-3} lighter than underlying mantle). They are 100 times more viscous than ambient mantle and their non-dimensional yield stress is 10 times larger than ambient mantle. The continental lithosphere that immediately surrounds the continent nuclei are 115 km thick and their buoyancy number is −0.3 (150 kg m^{-3} lighter than underlying mantle). They are 50 times more viscous than underlying mantle and they have a 10 times larger yield stress. The Tibetan region of Eurasia, prior to collision, is similarly thick and buoyant as the surrounding belts. This specific continental block is modelled here by 50 times more viscous material but 2.5 times larger yield stress than ambient mantle. The goal here is to parameterise efficient ductile deformation during the collision (Zhang et al., 2004). The parameters of the model are listed in Table 1.

The solution is computed with an energy contribution from the core of 25% of the total surface heat flux, the rest being internal heating. Both the surface and the bottom are isothermal, defining the temperature drop for the Rayleigh number Ra of 10^6, based on the reference viscosity defined above. The average surface velocity obtained with these parameters at statistical steady-state, without imposing surface velocities, is 1.2 cm y^{-1} when scaled with a thermal diffusivity of 10^{-6} m^2 s^{-1}. This is a factor of 3 lower than the Earth today. Unfortunately we are limited by computational cost to reach a realistic Ra that would produce Earth-like velocities. Since convective velocities are proportional to Ra$^{2/3}$, this factor of 3 means that we would need to increase Ra by a factor of 5 to reach appropriate Earth-like velocities with our approximation and keeping our dimensional value of thermal diffusivity. Another consequence of our low Rayleigh number is that convective structures are larger than for

Please cite this article as: N. Coltice et al., Interactions of scales of convection in the Earth's mantle, Tectonophysics (2017), http://dx.doi.org/10.1016/j.tecto.2017.06.028

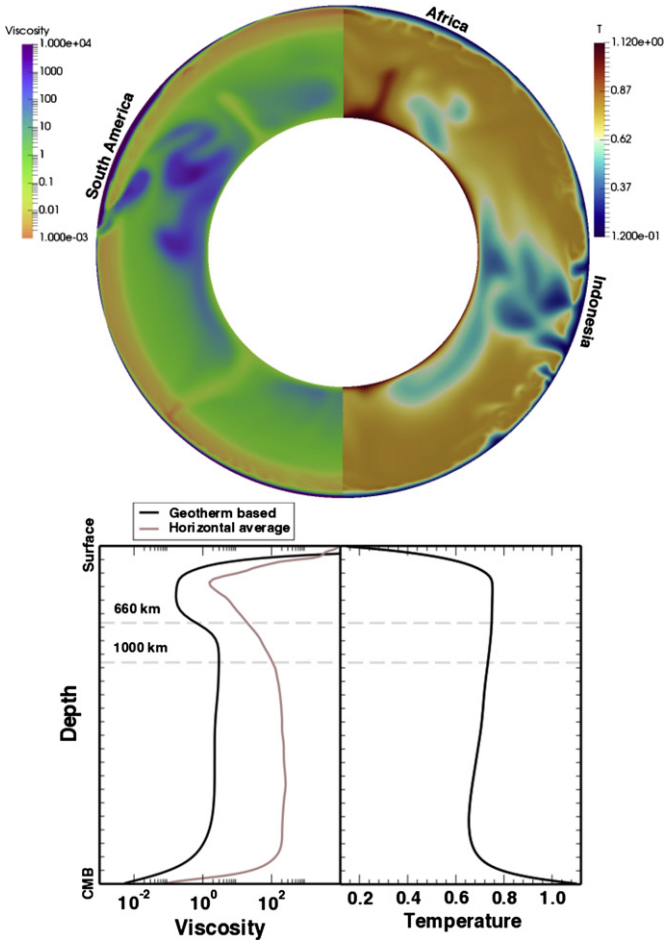

Fig. 1. Viscosity (left) and temperature (right) distributions within the final snapshot of the convection model, in non-dimensional units. Top: equatorial cross section to show typical viscosity and temperature distribution within the model. Bottom: viscosity profile corresponding to the geotherm on the right, and the horizontally averaged viscosity of the snapshot above (plumes and slabs contribute to these profiles).

the Earth. Hence, the reader should keep this in mind for the discussions on length scales. In the following, the dimensional time is also scaled in post processing in a way it is classically done: dimensional velocities produced by the model are multiplied by 3 and the model time is divided by 3, so that the values of velocities and time/age can directly be compared to the Earth for practical purposes.

2.2. Convection reconstruction

2.2.1. Methodology

In the lack of an applicable data assimilation tool that would generate initial conditions for the reconstruction of convective motions in the Earth up to the present-day, we use the following methodology: (1) build a temperature field for the continent configuration at 200 Ma, (2) impose plate velocities at the surface between 200 Ma and 0 Ma, updating the continent shapes at 80 Ma to account for the moderate changes which happened in terms of continental growth and deformation. Step 2 is straight forward, and has been done for nearly two decades (Bunge et al., 1998; McNamara and Zhong, 2005; Bower et al., 2015; Bello et al., 2015, among others). We consider here the plate kinematic model of Seton et al. (2012). Because convection in our model is less vigorous than on Earth, the imposed velocities at present-day are scaled to be consistent with the convective vigor of our model (Bello et al., 2015): the rms value of imposed present-day velocities equals the rms surface velocity of the model

Table 1
Non dimensional and dimensional parameters of the convection model, taking the following values for dimensionalisation producing the computed Rayleigh number.

Parameter	Non dimensional value	Dimensional value
Rayleigh number	10^6	
Heat production rate	20	4.610^{-12} W kg^{-1}
Top temperature	0.12	255 K
Basal temperature	1.12	2390 K
Reference density	1	4400 kg m^{-3}
Thermal expansivity	1	4.5 10^{-5} K^{-1}
Thermal diffusivity	1	10^{-6} m^2 s^{-1}
Thermal conductivity	1	4 W m^{-1} K^{-1}
Reference viscosity	1	10^{23} Pa s
Viscosity jump factor at 660 km	30	
Activation energy	8	142 kJ mol^{-1}
Yield stress at the surface	210^4	230 MPa
Yield stress depth derivative	2.5 10^5	1030 Pa m^{-1}
Continent nuclei viscosity factor	100	
Continent nuclei yield stress	210^5	2300 MPa
Buoyancy number for continent nuclei	−0.4	
Continent belts viscosity factor	50	
Continent belts yield stress	210^5	2300 MPa
Buoyancy for continent belt	−0.3	
Tibet viscosity factor	50	
Tibet yield stress	510^4	590 MPa
Buoyancy number for Tibet	−0.3	
Maximum viscosity cutoff	10^4	10^{27} Pa s

without imposed kinematics. Imposing plate motion history potentially helps impede the propagation of errors from initial conditions (Colli et al., 2015). A drawback is that artificial stresses are generated at the surface when kinematics are imposed as the surface boundary condition, contrary to more realistic free slip boundary conditions, or even better, a free surface (Lowman, 2011).

For Step 1 of the method, we have to make an arbitrary choice. We pick a temperature field from a computed dynamic evolution in which the continental configuration at 200 Ma is fixed. The advantage is that the solution is natural for the set of equations and parameters, respecting the statistical-steady state of the convecting system. The drawback is that nothing, except the position of the continents, comes from observations. We chose here a solution in which a subduction ring on the West side of Pangea exists, as well as subduction East of Africa, as shown in Fig. 2. These features are proposed in the reconstruction of Seton et al. (2012). Interactions between large-scale and small-scale convection exist in this self-organised convective system. The flow features we describe in the next section are similarly present in the calculations without imposed surface plate motions, where plate boundaries are self-generated through pseudo-plasticity. We share the data corresponding to the snapshot presented here, at the following internet address: https://osf.io/ee6sk/.

3. Results

3.1. Sublithospheric instabilities below the ocean floor

Sublithospheric instabilities start as cold drips sinking in networks from the base of the boundary layer beneath an oceanic plate as seen in Fig. 3. The cold drips are limited to the upper mantle. The jump in viscosity into the lower mantle precludes the existence of lower mantle smaller scale features. The small scale instabilities are organised in networks. They develop from undulations of the isotherms building up into sinking drips. Their onset age is variable from one oceanic region to another. Undulations of the isotherms can be apparent for seafloor ages around 40 Ma in these calculations, but drip-like instabilities characterizing small-scale convection only develop for ages larger than 60 Ma (see Fig. 4). This organisation of

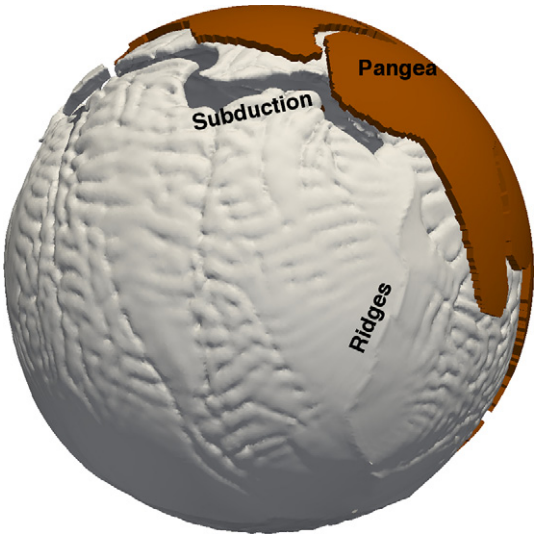

Fig. 2. Selected 3D view of initial condition of the model (200 Ma). Continental material is highlighted in brown. South America is visible on the left side. A cold isotherm corresponding to the base of the boundary layer shows the downwellings (large-scale convection) and the small-scale convection pattern (seen as undulations of the isotherm). This solution corresponds to a snapshot of the free convection calculation, without imposed plate motion and the surface. (For interpretation of the references to color in this figure legend, the reader is referred to the web version of this article.)

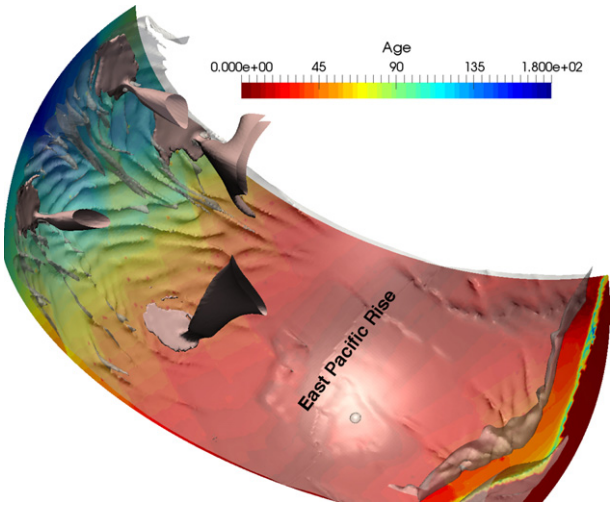

Fig. 4. 3D view of isosurface at isotherm T = 0.75 superimposed over a surface showing seafloor age in Ma. The view is from the interior of the mantle below a section of the Pacific. The isotherm T = 0.85 highlights hot plume conduits impacting the base of the boundary layer. The onset of instability corresponds to the existence of sinking drips.

dynamic structures is similar to those described by van Hunen et al. (2005). As mentioned above, these onset ages have been scaled for easier comparison with the Earth and regional models. As proposed by Dumoulin et al. (2005) instabilities frequently start along small circles aligned with fracture zones, and for younger-than-average seafloor age than average (Fig. 4). The evolution of seafloor spreading produces a complex pattern of isochrons in the ocean, which controls the onset of instabilities.

The networks of instabilities are approximately elongated in the direction of present-day spreading, and are influenced by far-field forces. Since instabilities develop beneath older seafloor, the geometry of isochrons organises the pattern of the network. In Fig. 3, the network pattern around Antarctica is more or less perpendicular to the ridge system, therefore networks tend to converge towards the continent. The change in spreading direction may influence the pattern too: a rare example of undulations of isotherms perpendicular to spreading exists along the ridge south of India (see Fig. 5), possibly related to the influence of the Indian plate slowing down through the collision with Eurasia. The instability networks close to the triple junction in the Indian Ocean shows interactions of spreading systems and thus less directional orientations, especially for the slower plates.

The shape of an instability is strongly influenced by the velocity of the plate: for a slowly moving plate negatively buoyant drips descent nearly vertically; the sink at an angle beneath faster plates. In the latter case, while the head of the drip sinks vertically, the location of onset of the instability is moved in the direction of the plate,

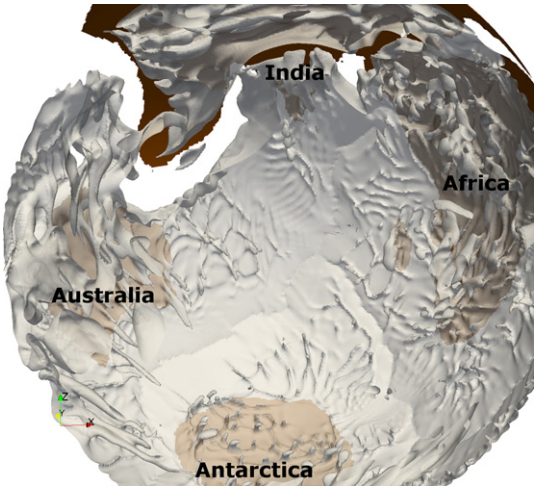

Fig. 3. 3D view from Earth's interior, centered on the Indian Ocean. The isotherm of T = 0.75 is isosurfaced (grey area), with continental material highlighted in brown. The isotherm is making fingers and drips that corresponds to small scale convective instabilities. Beneath Africa and Antarctica (slowly moving continents), they sink vertically, while they are sheared below Australia, which is moving fast. The same happens under oceanic areas. (For interpretation of the references to color in this figure legend, the reader is referred to the web version of this article.)

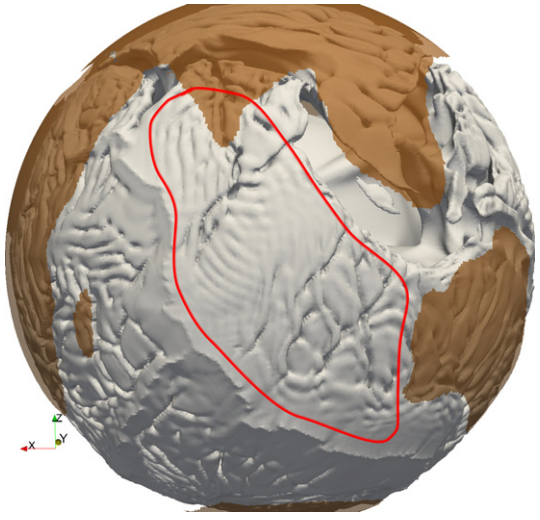

Fig. 5. Isosurfacing as in Fig. 2, focused on the Indian oceans. Instability networks, marked by folding of the isosurface show interactions with each other with the presence of convergent plate boundaries in the North. The area surrounded by a red line displays transverse undulations of the isotherm. (For interpretation of the references to color in this figure legend, the reader is referred to the web version of this article.)

Please cite this article as: N. Coltice et al., Interactions of scales of convection in the Earth's mantle, Tectonophysics (2017), http://dx.doi.org/10.1016/j.tecto.2017.06.028

producing the dip angle (see Fig. 3). Both the inclination of the velocity vector and the type of flow produced by small-scale convection depend on the ratio between the velocity of the plate and that of the cold instabilities. For a ratio smaller than 1, the cold drips sink vertically and generate a rotating velocity field that dominates the overall flow as depicted in Fig. 6. On the contrary, for a ratio larger than 1, the cold drips show a dip angle. Because the plate flow is faster than the sinking velocity of cold drips, the velocity field is undulating but remains in the direction of plate motion (see Fig. 6).

3.2. Plumes and small scale convection below the ocean floor

In the present-day snapshot, we identify 21 plumes, which influence the organisation of instabilities around them. Plume locations are model plume locations and do not necessarily agree with real plume locations. Plumes generate a wake pointing in the direction of plate motion. It consists of a hotter channel that modestly thermally rejuvenates the overlying seafloor: with the viscosity contrast used here, the thinning of the thermal boundary layer is weak, as proposed by Monnereau et al. (1993). The plate-scale pattern of small-scale convection is self-organised around plumes in networks, elongated in the direction of spreading (see Fig. 7). Within the plume wake, small scale instabilities develop as cold drips (see Fig. 8) sinking from V-shape undulations perpendicular to the direction of plate motion (see Fig. 7). These structures are similar to those described by Moore et al. (1998), Thoraval et al. (2006) or Ballmer et al. (2011). The older the seafloor at the location of plume impact, the stronger the intensity is of small-scale convection downstream of the plume ponding location. Plumes reaching the boundary layer closer to the East Pacific rise (thus, young oceanic lithosphere) do not display the strong pattern of small-scale convection seen for plumes further away beneath older oceanic lithosphere (Fig. 7).

We thus observe channel-like structures beneath the seafloor: (a) hotter ones correspond to the wake of plumes with small-scale instabilities developing downstream especially if the seafloor is old, and (b) colder channels focus instabilities between plume wakes, initiating upstream of plumes impacting lithosphere older than 60 Ma

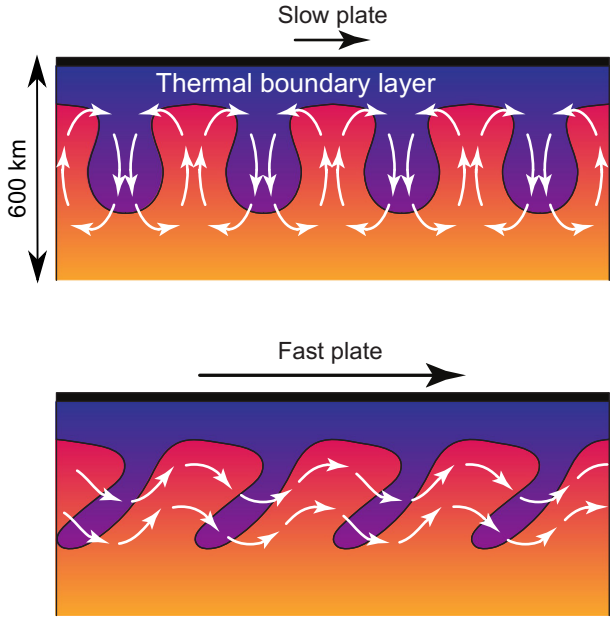

Fig. 6. Schematic cross section view of the velocity field produced in the upper mantle by the interaction of plates and small scale convection. Cold instabilities are represented in purple. Top: slow plate velocity relative to sinking velocity of cold drips. Bottom: fast plate velocity relative to cold drips. (For interpretation of the references to color in this figure legend, the reader is referred to the web version of this article.)

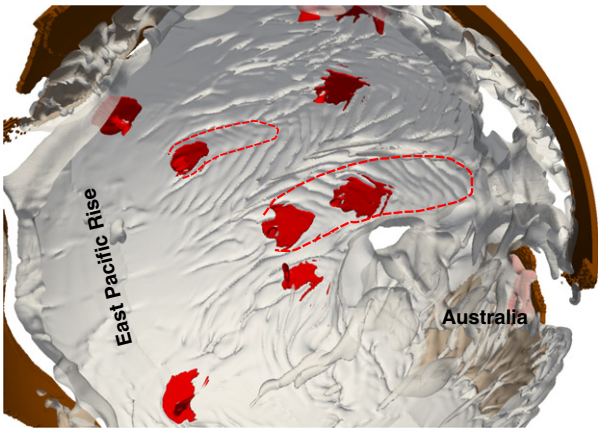

Fig. 7. 3D view from the inside of the sphere, of plumes and small scale convection interactions below the Pacific seafloor. Iso-surfacing as in Fig. 2. Instability networks, marked by folding of the isotherm show interactions with plumes highlighted by red isosurfacing at isotherm at 0.85 (cut below 600 km). Red dashed lines highlight some channels in the wake of plumes. (For interpretation of the references to color in this figure legend, the reader is referred to the web version of this article.)

(Fig. 7). The width of the wakes is typically on the order of 1000 km here.

3.3. Sublithospheric convection below the continents

Below continents, small-scale instabilities are also organised in networks from which cold drips develop. The boundary layer beneath continents is thicker than the continental lid itself, reaching here 300 km. Its base is defined as the location where the temperature "departs significantly from the isentropic profile" as in Michaut et al. (2007). Since continents are in general the portion of plates that have the older thermal ages, the thermal boundary layer beneath them is the most unstable. The networks and the dip angle of the instabilities are in the same direction as plate motion. It is particularly clear for Australia in Fig. 3, which is moving fast, but also in Fig. 9 for Eurasia and the northwest of Africa which are slower moving plates. For continents like the southern part of Africa or Antarctica, the pattern is complex because several spreading systems surrounding them are involved. The boundaries between oceans and continents tend to localize the onset of instabilities, see for instance the northwest of Africa or south of Australia in Fig. 9. This is consistent with earlier findings involving edge-driven convection (King and Ritsema, 2000). At the edges of continents, the networks develop mostly perpendicularly to the ocean-continent boundary, and move towards a more complex planform in the interior. Close to a subduction zone, the patterns changes and tend to align with the trench, as with India in Fig. 9. The presence of plumes beneath continents has a similar impact as under oceans: they reheat the lithosphere over the region of plume ponding, depending on the power of the plume (see the two plumes beneath Africa, and that close to its equatorial edge

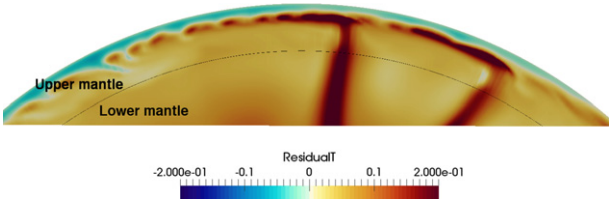

Fig. 8. Non-dimensional residual temperature in a cross section through plumes wakes in the Pacific. The residual temperature is the deviation from the average temperature profile. The scale is saturated below −0.2 and over 0.2 to highlight small scale convection. The residual temperature in the plume exceeds 0.2.

Please cite this article as: N. Coltice et al., Interactions of scales of convection in the Earth's mantle, Tectonophysics (2017), http://dx.doi.org/10.1016/j.tecto.2017.06.028

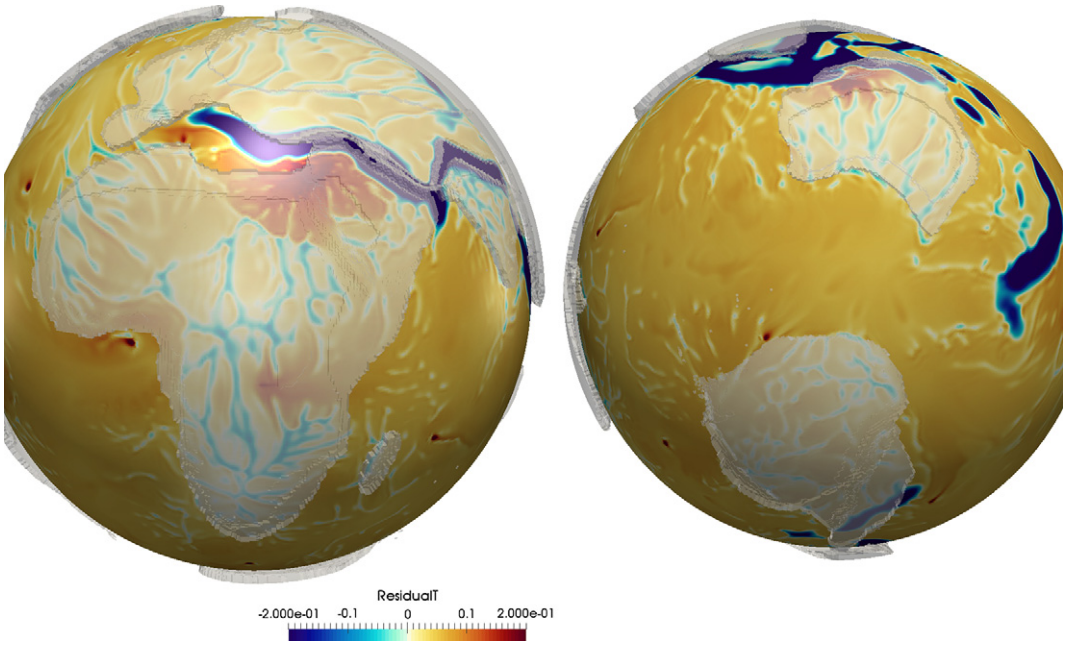

Fig. 9. Hemispheric views of the non-dimensional residual temperature at 310 km depth (base of the thermal boundary layer beneath continents). The residual temperature is the deviation from the average temperature profile. The scale is saturated below −0.2 and over 0.2 to highlight small scale convection under continents. The residual temperatures within plumes and slabs exceed the scale.

in Fig. 9). The small-scale convection planform beneath continents combines the effects of convective instabilities described by Fourel et al. (2013) (spokes perpendicular to the boundaries and polygonal cells in the interior) with those of plate motions, subduction and plumes.

3.4. Scales of convection

To characterize the scales of small-scale convection, we first choose the inclination of the velocity as the relevant field, defined as the angle between computed velocity and the horizontal. A negative inclination indicates a sinking flow, and a positive inclination indicates rising flow. Small-scale convection produces rolls (linear alternation of positive and negative inclination) and sinking drops (circular patches of negative inclinations). Temperature and velocity field variations tend to highlight plumes and downwellings, and thus are not as relevant as the inclination of velocity. We compute the power spectrum of the inclination of the velocity up to degree 350, ~100 km (see Fig. 10). Within the whole domain, the dominating structures are for the low spherical harmonic degrees, corresponding to the large-scale flow marked by the subduction rings. However, the expanded power spectrum (Fig. 10) of the inclination shows a substantial signal for degrees 20 up to 200 between the base of the boundary layer below oceans and 700 km depth (the top of the lower mantle). Deeper in the mantle, the flow is limited to harmonic degrees between 1 and 50, with most of the power being in the first 20°.

Harmonic degrees lower than 50 show a structure at 350 km depth which corresponds mostly to sinking slabs (Fig. 11). We also notice elongated structures in the direction of plate motion in the wake of computed plumes in the Pacific. Harmonic degrees 50 to 200 capture the organisation of sublithospheric instabilities (Fig. 12). The structure of networks appears as rolls parallel to plate motion except in area of compressive stresses where networks are perpendicular to plate motion (below Central Asia and close to subduction zones).

4. Discussion

4.1. From the model to the Earth

The model presented in this study is not aimed at directly reproducing the Earth. First, the physics of mantle convection is approximated as discussed earlier. Also, since initial conditions and rheological parameters are not perfectly known, the computed temperature and flow fields have intrinsic errors (Bello et al., 2014, 2015). Imposing velocity conditions at the surface produces errors as well, because

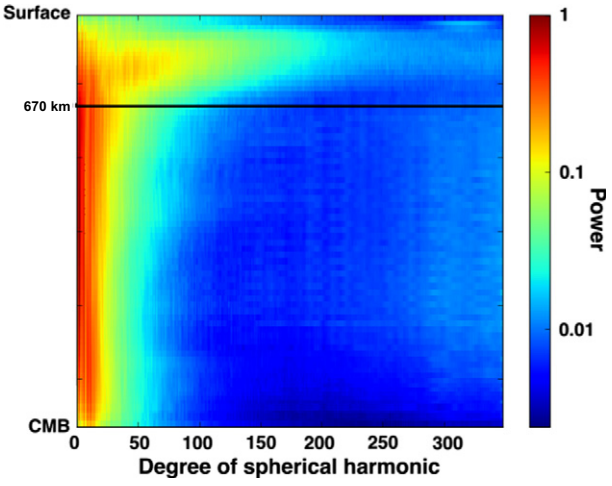

Fig. 10. Power spectrum of the inclination of the velocity field. The local changes of the inclination of the velocity field in the upper mantle display interactions of scales between spherical harmonic degrees 1 and 200, while the lower mantle shows interactions of scales restricted to lower harmonic degrees.

Please cite this article as: N. Coltice et al., Interactions of scales of convection in the Earth's mantle, Tectonophysics (2017), http://dx.doi.org/10.1016/j.tecto.2017.06.028

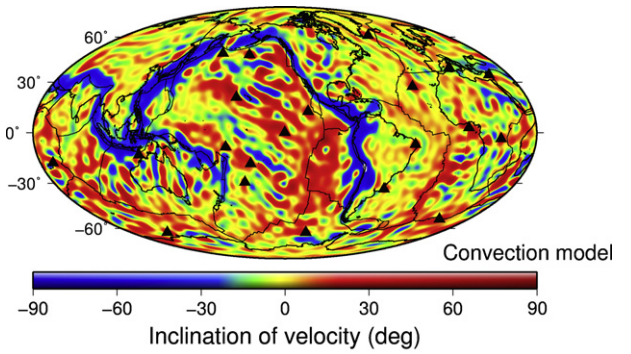

Fig. 11. Inclination of the velocity field from degree 1 to 50 at 350 km depth. The locations where plumes hit the cold boundary layer are plotted with black triangles. Red means the flow is going upward, while blue means a downward flow. The wakes of plumes, especially in the Pacific are observed at these scales. (For interpretation of the references to color in this figure legend, the reader is referred to the web version of this article.)

the plate reconstructions have intrinsic uncertainties, and because the method generates artificial stresses at the boundary (Lowman, 2011). Data assimilation strategies, using plate reconstructions as a data to match would solve both of the latter problems and the initial condition issue, but these methods are under development (Bocher et al., 2016, 2017).

A lower Rayleigh number than the Earth is a substantial limitation for the interpretations in terms of length-scales. Indeed, the thickness of the boundary layer defines a sort of minimum length scale for convective structures. Since in this model the boundary layer below oceans is consistently 200 km thick due to the lower convective vigor of our model compared to Earth, length scales smaller than the thickness of the boundary layer barely exists. However, on Earth, the oceanic lithosphere is about twice as thin. Therefore, the power of the inclination of the velocity could thus extend to greater harmonic degrees, and the size of the plume channels could be smaller by a factor of two as well. Smaller-scale features than 200 km for Earth-like conditions potentially exist but remain conjectural at this point.

The rheological model for the oceanic and continental lithosphere we used here is reduced to a simple pseudo-plastic approximation for the whole layer. Improving the models to take into account the variety of deformation mechanisms, the lateral and vertical heterogeneities within the lithosphere (Burov et al., 1998; Burov, 2011), and to include elasticity, which can accelerate or impede the development of instabilities (Burov and Molnar, 2008), is fundamental for evaluation of the influence of small-scale convection on small time scales and regional tectonics (Burov, 2007).

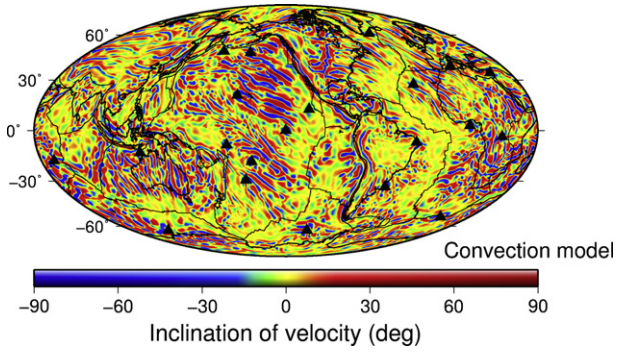

Fig. 12. Inclination of the velocity field from degree 50 to 200 at 350 km depth. The locations where plumes hit the cold boundary layer are plotted with black triangles. Red means the flow is going upward, while blue means a downward flow. The networks of instabilities (especially in between plume wakes) are observed at these scales. (For interpretation of the references to color in this figure legend, the reader is referred to the web version of this article.)

Despite these limitations, the dynamics of small-scale convection in relationship to plumes and subduction presented here, provides valuable insight on small-scale instabilities on Earth. Indeed, the development of small-scale instabilities has only minor dependency on several important phenomena, such as: a factor of five change of the Rayleigh number (as long as the yielding parameters are changed to keep the model in the same tectonic regime); the contribution of core heat flow unless core heating becomes dominant; uncertainties in deep mantle properties like composition; and on the method producing Earth-like kinematics at the surface (we made similar observations on a model without imposed velocities). We expect that the width of plume wakes and the size of cold instabilities could be smaller by a factor of two maximum on our planet, with the global organisation of the flow being consistent with the models presented here.

4.2. Potential seismic signatures of plume-lithosphere interaction and sublithospheric instabilities

Small-scale convective structures are intrinsically difficult to image with seismological methods. First, the length scales of small-scale convection are short, while those of recent tomographic imaging below the oceans reach 600 km in the uppermost 200 km, but then increases rapidly to ∼2500 km in the transition zone (Becker and Boschi, 2002; Debayle and Ricard, 2012; Meschede and Romanowicz, 2015). Also, the seismic anomalies associated with the structures presented here are expected to be small since the temperature anomalies are < 50 K. Furthermore, the temperature gradients are also small. Forward modeling approaches can image smaller scale structures, but usually suffer from an inability to model structure over global expanses. Therefore, unequivocal detection is difficult. Therefore, we propose here ways to detect indirect evidence of small-scale convection beneath plates.

We observed that the interaction of a plume with the lithosphere produces wakes in the direction of plate motion, in which small-scale convection can develop downstream if the seafloor is old at the place of plume impact. Small-scale convection also develops upstream and around the wakes. Therefore, the regions in between wakes of plumes accumulate sinking cold instabilities. Some authors using regional models also suggest a contribution from a plume's return flow to cold "downwelling curtains" (Moore et al., 1998). Since large-scale and small-scale flow are interacting in our model, this return flow may be distributed over the whole globe. In the end, the curtains are difficult to identify from small-scale convection (some plumes in Fig. 7 do not show curtains at all). Using waveform tomography, French et al. (2013) proposed channel-like structures in the asthenosphere that are consistent with the alternation of hot wakes of plumes with colder regions between wakes. French et al. (2013) present wakes of about 1000 km in width, and extending in the direction of plate motion over thousands of kilometers. These wavelengths are consistent with our model predictions. The channels do not represent a detection of small-scale convection strictly speaking, but the coalescence of small-scale instabilities between plume wakes generate an even stronger contrast with the hot channels than if there were no small-scale convection.

The interactions between plume ponding and small scale convection within the plume wakes are likely to disturb an otherwise simpler pattern of anisotropy beneath fast-moving plates. Maggi et al. (2006) demonstrated that if fast anisotropic directions are not resolved due to short-scale azimuthal variations, the region where anisotropy is disturbed can be detected. Such plume-related perturbations were first detected behind hotspots in the Pacific Ocean

by Maggi et al. (2006) and are observed at the bottom of the oceanic lithosphere in more recent seismic models (Debayle et al., 2016, see Fig. 13). As observed as in Fig. 13, only plumes impacting seafloor older than 70 Ma in the Pacific display a wake of perturbed anisotropy direction. Such an observation is consistent with the behavior depicted in our model. The pattern of disturbance downstream plumes on Earth is about 1000 km in lateral scale, similar to the channels described by French et al. (2013).

The direct detection of small-scale instabilities below plates is not presently resolvable using classical tomographic approaches, because the wavelengths are too short. However, our results suggest the presence of different patterns of azimuthal seismic anisotropy below slow and fast plates. Indeed, instabilities beneath fast plates are stretched in the direction of the motion of the plate. As the size of these instabilities are smaller than the wavelengths of the seismic waves used to image the upper mantle, we expect an equivalent azimuthal anisotropy in the same direction as plate motion. For slower plates, instabilities sink vertically producing distributed heterogeneities that may not generate equivalent anisotropy. This reduced directional organisation is consistent with the work of Husson et al. (2015). These hypotheses could be consistent with the seismic azimuthal anisotropy distribution of Debayle and Ricard (2013), showing anisotropy is parallel to fast plates velocities below the base of the lithosphere, whereas the relationship between azimuthal anisotropy and plate motion remains diffuse below slower plates. However, this hypothesis has to be evaluated in a more comprehensive study, computing both the effects of intrinsic anisotropy, produced by lattice preferred orientations, and extrinsic anisotropy produced by directional temperature anomalies at smaller length scales than that of seismic waves used for tomographic inversions (Fichtner et al., 2013; Bodin et al., 2015).

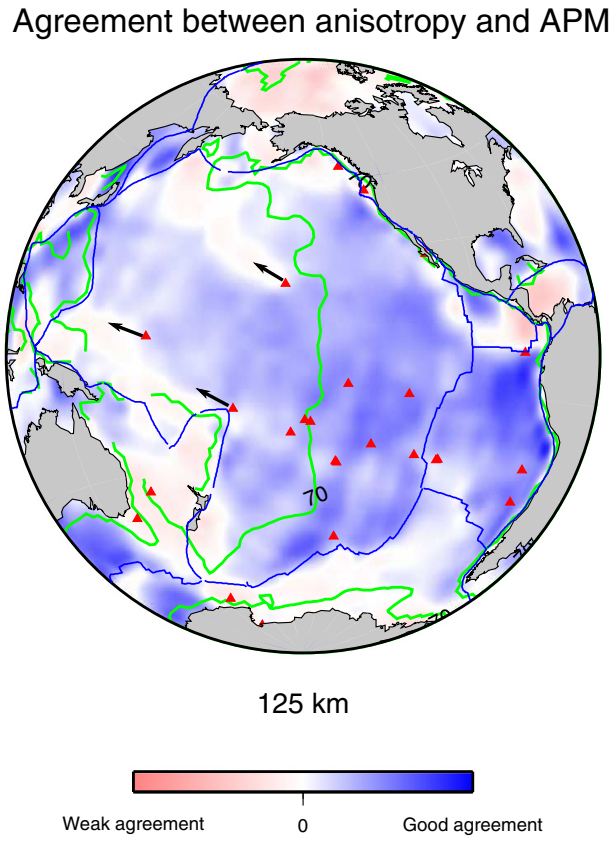

Fig. 13. Agreement at a depth of 125 km between fast SV-wave anisotropy directions (Debayle et al., 2016) and absolute plate motion (APM) calculated from NUVEL1 (DeMets et al., 1994) in the no-net rotation reference frame. The parameter $A\cos(2\alpha)$, where A is the amplitude of the fast SV-wave vector and α the angle between APM and fast SV-wave azimuth, is shown. Good agreement (parallelism of the two vectors) is represented in blue, weak agreement in white and bad agreement (orthogonality) in red. The color scales are symmetric, adapted to cover the full range of values, the zero value corresponds in some case to a zero anisotropy or more often to an angle of 45° between fast anisotropy and APM. The green lines indicate the 70 Ma isochron. The agreement between anisotropy and APM is disturbed in a region forming a wake in the direction of plate motion. The plate motion direction in the no-net reference frame is indicated for 3 hotspots (Hawaii, Caroline, Samoa) for which such disturbances are clearly detected. These hotspots are located on sea floor age >70 Ma, the age at which the onset of small-scale convection is commonly observed (Stein et al., 1994, e.g.). (For interpretation of the references to color in this figure legend, the reader is referred to the web version of this article.)

5. Conclusions

Computing a global 3D spherical geodynamic model with large lateral variations of viscosities, we generate convective flow with a variety of scales. Small-scale convection develops in the upper mantle only, producing networks of cold sinking instabilities. Instabilities are drip-shaped, and dominantly influenced by the velocity of plates. Indeed, fast plates are accompanied with instabilities that are dipping in the opposite direction of plate motion, while slow plates display vertically sinking instabilities. The typical wavelength of the networks of instabilities is on the order of 200 km in the geodynamic models, and it is expected to be around 100 km on Earth. Because of the small temperature gradients and the small size of these features, they may not be easily detected by conventional seismic methods at global scale. However, we suggest that the pattern of azimuthal anisotropy observed beneath the lithosphere could be in close relationship with the temperature distribution and type of flow generated by these instabilities. However, we do not provide a quantitative assessment of that hypothesis here.

The networks of cold instabilities presented here are usually organised along the direction of spreading. Subduction tends to align the networks parallel to trenches. Also, the ocean-continent boundary can localize the onset of instabilities, and the geometry of continents controls the pattern of small-scale convection beneath them. Plumes focus the instabilities in between their wakes, while generating small-scale convection in the hot channels downstream, below seafloor older than 50–70 Ma. The typical width of wakes is of the order of 1000 km in the model, therefore on Earth they would be larger than 500 km. These features are consistent with the finger-like structures found in the tomographic models of French et al. (2013). Cold instabilities occur between the wakes of plumes. We propose that the interactions between plume ponding below old seafloor and small-scale convection within the plume wakes could perturb the azimuthal anisotropy of SV waves relative to the regional pattern, consistent with seismic anisotropy in the Pacific (Maggi et al., 2006).

Acknowledgments

We thank Barbara Romanowicz, Maxim Ballmer and Philippe Agard for comments and reviews that profoundly helped improve the manuscript. The research leading to these results has received funding from the European Research Council within the framework of the SP2-Ideas Program ERC-2013-CoG, under ERC grant agreement 617588. Calculations were performed at P2CHPD Lyon. We thank Maëlis Arnould for the automatic detection of plumes used in Figs. 11 and 12. We thank Vincent Perrier for helping on Fig. 6.

References

Ballmer, M., Ito, G., Van Hunen, J., Tackley, P., 2011. Small-scale convection induces spatio-temporal variability in Hawaiian volcanism. Nat. Geosci. 4, 457–460.
Ballmer, M., Van Hunen, J., Ito, G., Tackley, P., Bianco, T., 2007. Non-hotspot volcano chains originating from small-scale sublithospheric convection. Geophys. Res. Lett. 34, L23310.

Becker, T.W., Boschi, L., 2002. A comparison of tomographic and geodynamic mantle models. Geochem. Geophys. Geosyst. 3,

Bello, L., Coltice, N., Rolf, T., Tackley, P.J., 2014. On the predictability limit of convection models of the Earth's mantle. Geochem. Geophys. Geosyst. 15, 2319–2328.

Bello, L., Coltice, N., Tackley, P.J., Müller, R.D., Cannon, J., 2015. Assessing the role of slab rheology in coupled plate-mantle convection models. Earth Planet. Sci. Lett. 430, 191–201.

Bocher, M., Coltice, N., Fournier, A., Tackley, P., 2016. A sequential data assimilation approach for the joint reconstruction of mantle convection and surface tectonics. Geophys. J. Int. 204, 200–214.

Bocher, M., Fournier, A., Coltice, N., 2017. Ensemble Kalman filter for the reconstruction of the Earth's mantle circulation. Nonlinear Process. Geophys. under review.

Bodin, T., Capdeville, Y., Romanowicz, B., Montagner, J.-P., 2015. Interpreting radial anisotropy in global and regional tomographic models. The Earth's Heterogeneous Mantle. Springer., pp. 105–144.

Boutilier, R., Keen, C., 1999. Small-scale convection and divergent plate boundaries. J. Geophys. Res. Solid Earth 104, 7389–7403.

Bower, D.J., Gurnis, M., Flament, N., 2015. Assimilating lithosphere and slab history in 4-d Earth models. Phys. Earth Planet. Int. 238, 8–22.

Bunge, H.-P., Richards, M., Lithgow-Bertelloni, C., Baumgardner, J., Grand, S., Romanowicz, B., 1998. Time scales and heterogeneous structure in geodynamic Earth models. Science 280, 91–95.

Bunge, H.-P., Richards, M.A., Baumgardner, J.R., et al. 1996. Effect of depth-dependent viscosity on the planform of mantle convection. Nature 379, 436–438.

Burov, E., 2007. The role of the gravitational instabilities, the density structure and the extension rate in the evolution of slow continental margins. Geol. Soc. Spec. Publ. 282, 139–156.

Burov, E., Jaupart, C., Mareschal, J., 1998. Large-scale crustal heterogeneities and lithospheric strength in cratons. Earth Planet. Sci. Lett. 164, 205–219.

Burov, E., Molnar, P., 2008. Small and large-amplitude gravitational instability of an elastically compressible viscoelastic maxwell solid overlying an inviscid incompressible fluid: dependence of growth rates on wave number and elastic constants at low Deborah numbers. Earth Planet. Sci. Lett. 275, 370–381.

Burov, E.B., 2011. Rheology and strength of the lithosphere. Mar. Pet. Geol. 28, 1402–1443.

Christensen, U.R., 1984. Convection with pressure and temperature dependent non-Newtonian rheology. Geophys. J. R. Astron. Soc. 77, 242–284.

Colli, L., Bunge, H.-P., Schuberth, B.S., 2015. On retrodictions of global mantle flow with assimilated surface velocities. Geophys. Res. Lett. 42, 8341–8348.

Davaille, A., Jaupart, C., 1994. Onset of thermal convection in fluids with temperature-dependent viscosity: application to the oceanic mantle. J. Geophys. Res. Solid Earth 99, 19853–19866.

Davies, D.R., Goes, S., Davies, J.H., Schuberth, B., Bunge, H.-P., Ritsema, J., 2012. Reconciling dynamic and seismic models of Earth's lower mantle: the dominant role of thermal heterogeneity. Earth Planet. Sci. Lett. 353, 253–269.

Debayle, E., Dubuffet, F., Durand, S., 2016. An automatically updated S-wave model of the upper mantle and the depth extent of azimuthal anisotropy. Geophys. Res. Lett. 43, 674–682.

Debayle, E., Ricard, Y., 2012. A global shear velocity model of the upper mantle from fundamental and higher Rayleigh mode measurements. J. Geophys. Res. Solid Earth 117, B10308.

Debayle, E., Ricard, Y., 2013. Seismic observations of large-scale deformation at the bottom of fast-moving plates. Earth Planet. Sci. Lett. 376, 165–177.

DeMets, C., Gordon, R.G., Argus, D.F., Stein, S., 1994. Effect of recent revisions to the geomagnetic reversal time scale on estimates of current plate motions. Geophys. Res. Lett. 21, 2191–2194.

Dumoulin, C., Doin, M.-P., Arcay, D., Fleitout, L., 2005. Onset of small-scale instabilities at the base of the lithosphere: scaling laws and role of pre-existing lithospheric structures. Geophys. J. Int. 160, 344–356.

Fichtner, A., Kennett, B.L., Trampert, J., 2013. Separating intrinsic and apparent anisotropy. Phys. Earth Planet. Inter. 219, 11–20.

Fleitout, L., Moriceau, C., 1992. Short-wavelength geoid, bathymetry and the convective pattern beneath the Pacific Ocean. Geophys. J. Int. 110, 6–28.

Foley, B.J., Becker, T.W., 2009. Generation of plate-like behavior and mantle heterogeneity from a spherical, viscoplastic convection model. Geochem. Geophys. Geosyst. 10,

Fourel, L., Milelli, L., Jaupart, C., Limare, A., 2013. Generation of continental rifts, basins, and swells by lithosphere instabilities. J. Geophys. Res. 118, 3080–3100.

French, S., Lekic, V., Romanowicz, B., 2013. Waveform tomography reveals channeled flow at the base of the oceanic asthenosphere. Science 342, 227–230.

Grand, S.P., van der Hilst, R.D., Widiyantoro, S., 1997. High resolution global tomography: a snapshot of convection in the Earth. Geol. Soc. Am. Today 7,

Guillou, L., Jaupart, C., 1995. On the effect of continents on mantle convection. J. Geophys. Res. Solid Earth 100, 24217–24238.

Gurnis, M., 1988. Large-scale mantle convection and the aggregation and dispersal of supercontinents. Nature 332, 695–699.

Hasterok, D., Chapman, D., Davis, E., 2011. Oceanic heat flow: implications for global heat loss. Earth Planet. Sci. Lett. 311, 386–395.

Haxby, W.F., Weissel, J.K., 1986. Evidence for small-scale mantle convection from Seasat altimeter data. J. Geophys. Res. Solid Earth 91, 3507–3520.

Hayn, M., Panet, I., Diament, M., Holschneider, M., Mandea, M., Davaille, A., 2012. Wavelet-based directional analysis of the gravity field: evidence for large-scale undulations. Geophys. J. Int. 189, 1430–1456.

Huang, J., Zhong, S., van Hunen, J., 2003. Controls on sublithospheric small-scale convection. J. Geophys. Res. Solid Earth 108,

Husson, L., Yamato, P., Bezos, A., 2015. Ultraslow, slow, or fast spreading ridges: arm wrestling between mantle convection and far-field tectonics. Earth Planet. Sci. Lett. 429, 205–215.

Idrissi, H., Bollinger, C., Boioli, F., Schryvers, D., Cordier, P., 2016. Low-temperature plasticity of olivine revisited with in situ tem nanomechanical testing. Sci. Adv. 2, e1501671.

Kageyama, A., Sato, T., 2004. "The Yin-Yang Grid": an overset grid in spherical geometry. Geochem. Geophys. Geosyst. 5,

King, S.D., Ritsema, J., 2000. African hot spot volcanism: small-scale convection in the upper mantle beneath cratons. Science 290, 1137–1140.

Korenaga, J., Jordan, T.H., 2003. Physics of multiscale convection in Earth's mantle: onset of sublithospheric convection. J. Geophys. Res. Solid Earth 108,

Lin, P.-Y.P., Gaherty, J.B., Jin, G., Collins, J.A., Lizarralde, D., Evans, R.L., Hirth, G., 2016. High-resolution seismic constraints on flow dynamics in the oceanic asthenosphere. Nature 535, 538–541.

Lowman, J.P., 2011. Mantle convection models featuring plate tectonic behavior: an overview of methods and progress. Tectonophys 510, 1–16.

Maggi, A., Debayle, E., Priestley, K., Barruol, G., 2006. Azimuthal anisotropy of the Pacific region. Earth Planet. Sci. Lett. 250, 53–71.

Mallard, C., Coltice, N., Seton, M., Müller, R.D., Tackley, P.J., 2016. Subduction controls the distribution and fragmentation of Earth's tectonic plates. Nat. Adv. Online Publ.

Marquart, G., 2001. On the geometry of mantle flow beneath drifting lithospheric plates. Geophys. J. Int. 144, 356–372.

McKenzie, D.P., 1967. Some remarks on heat flow and gravity anomalies. J. Geophys. Res. 72, 6261–6273.

McNamara, A.K., Zhong, S., 2005. Thermochemical structures beneath Africa and the Pacific Ocean. Nature 437, 1136–1139.

Meschede, M., Romanowicz, B., 2015. Lateral heterogeneity scales in regional and global upper mantle shear velocity models. Geophys. J. Int. 200, 1078–1095.

Michaut, C., Jaupart, C., Bell, D., 2007. Transient geotherms in Archean continental lithosphere: new constraints on thickness and heat production of the subcontinental lithospheric mantle. J. Geophys. Res. 112,

Monnereau, M., Rabinowicz, M., Arquis, E., 1993. Mechanical erosion and reheating of the lithosphere: a numerical model for hotspot swells. J. Geophys. Res. 98, 809–823.

Moore, W.B., Schubert, G., Tackley, P., 1998. Three-dimensional simulations of plume-lithosphere interaction at the Hawaiian swell. Science 279, 1008–1011.

Parsons, B., Sclater, J.G., 1977. An analysis of the variation of ocean floor bathymetry and heat flow with age. J. Geophys. Res. 82, 803–827.

Ricard, Y., Richards, M., Lithgow-Bertelloni, C., Le Stunff, Y., 1993. A geodynamic model of mantle density heterogeneity. J. Geophys. Res. 98, 21895–21909.

Richter, F.M., Parsons, B., 1975. On the interaction of two scales of convection in the mantle. J. Geophys. Res. 80, 2529–2541.

Rolf, T., Coltice, N., Tackley, P., 2012. Linking continental drift, plate tectonics and the thermal state of the Earth's mantle. Earth Planet. Sci. Lett. 351, 134–146.

Rudolph, M.L., Lekić, V., Lithgow-Bertelloni, C., 2015. Viscosity jump in Earth's mid–mantle. Science 350, 1349–1352.

Seton, M., Müller, R., Zahirovic, S., Gaina, C., Torsvik, T., Shephard, G., Talsma, A., Gurnis, M., Turner, M., Maus, S., et al. 2012. Global continental and ocean basin reconstructions since 200 Ma. Earth-Sci. Rev. 113, 212–270.

Sleep, N.H., 2011. Seismically observable features of mature stagnant-lid convection at the base of the lithosphere: some scaling relationships. Geochem. Geophys. Geosys. 12,

Solomatov, V., 2004. Initiation of subduction by small-scale convection. J. Geophys. Res. Solid Earth 109,

Stein, R.S., King, G.C.P., Lin, J., 1994. Stress triggering of the 1994 M = 6.7 Northridge, California, earthquake by its predecessors. Science 265, 1432–1435.

Tackley, P.J., 2008. Modelling compressible mantle convection with large viscosity contrasts in a three-dimensional spherical shell using the yin-yang grid. Phys. Earth Planet. Inter. 171, 7–18.

Thoraval, C., Tommasi, A., Doin, M.-P., 2006. Plume-lithosphere interaction beneath a fast moving plate. Geophys. Res. Lett. 33,

Tosi, N., Stein, C., Noack, L., Httig, C., Maierová, P., Samuel, H., Davies, D.R., Wilson, C.R., Kramer, S.C., Thieulot, C., Glerum, A., Fraters, M., Spakman, W., Rozel, A., Tackley, P.J., 2015. A community benchmark for viscoplastic thermal convection in a 2-D square box. Geochem. Geophys. Geosyst. 16, 2175–2196.

Van Heck, H., Tackley, P., 2008. Planforms of self-consistently generated plates in 3D spherical geometry. Geophys. Res. Lett. 35,

van Hunen, J., Zhong, S., Shapiro, N.M., Ritzwoller, M.H., 2005. New evidence for dislocation creep from 3-D geodynamic modeling of the Pacific upper mantle structure. Phys. Earth Planet. Inter. 238, 146–155.

Yamazaki, D., Karato, S.-i., 2001. Some mineral physics constraints on the rheology and geothermal structure of Earth's lower mantle. Am. Mineral. 86, 385–391.

Zhang, N., Zhong, S., Leng, W., Li, Z.-X., 2010. A model for the evolution of the Earth's mantle structure since the Early Paleozoic. J. Geophys. Res. Solid Earth 115,

Zhang, P.-Z., Shen, Z., Wang, M., Gan, W., Bürgmann, R., Molnar, P., Wang, Q., Niu, Z., Sun, J., Wu, J., et al. 2004. Continuous deformation of the Tibetan Plateau from global positioning system data. Geology 32, 809–812.

Zhong, S., Zuber, M.T., Moresi, L., Gurnis, M., 2000. Role of temperature-dependent viscosity and surface plates in spherical shell models of mantle convection. J. Geophys. Res. Solid Earth 105, 11063–11082.

Please cite this article as: N. Coltice et al., Interactions of scales of convection in the Earth's mantle, Tectonophysics (2017), http://dx.doi.org/10.1016/j.tecto.2017.06.028